THE EFFECT OF PULSE CHARGING ON THE CYCLE-LIFE PERFORMANCE OF ZINC/NICKEL OXIDE CELLS

M H KATZ*, T C ADLER, F R MCLARNON** and E J CAIRNS

Applied Science Division, Lawrence Berkeley Laboratory and Department of Chemical Engineering, University of California, Berkeley, CA 94720 (U S A)

(Received March 16, 1987, in revised form July 10, 1987)

Summary

The effect of various pulse-charging regimens on the lifetime and performance of model 1 5 A h zinc/nickel oxide cells has been determined. Charging frequencies ranged from 8.3 to 60 Hz, peak charging current densities ranged from 3.9 to 40.6 mA cm^{-2}, and charge off-time/on-time ratios varied from 1/1 to 9/1. All cells were subjected to 2 5 h constant-power discharges to 100% of the nickel oxide electrode capacity. The best cycle-life performance was obtained using a pulse-charging regimen of 30 ms *on*/90 ms *off* with 16 mA cm^{-2} peak current density. The cell lost capacity at a rate of 0.21%/cycle, which represents a two- to three-fold improvement compared with the rate of capacity loss for cells charged using constant current

Introduction

The secondary Zn/KOH/NiOOH cell offers attractive specific energy and specific power characteristics for demanding applications such as electric vehicles. Unsatisfactory cycle life is the major shortcoming of this secondary cell [1], and the Zn electrode is the focus of most research efforts to improve its lifetime Four processes are known to seriously compromise Zn electrode performance Zn redistribution (shape change), densification, passivation and dendrite formation [2]. Zinc redistribution is linked to the high solubility of its discharge products in the KOH electrolyte [3] Successful attempts to reduce this Zn solubility include the use of additives in the electrode [4, 5] or in the electrolyte [6 - 8]. The rate of dendrite shorting has been reduced by sealing the cells and by the development of separators that more effectively slow the rate of dendrite penetration [9]

An electric vehicle battery is typically subjected to a variable load due to the transient nature of vehicle acceleration and deceleration, steep road

*Present address Rubenslei 6, 2018 Antwerp, Belgium

**Author to whom correspondence should be addressed

0378-7753/88/$3 50

grades, etc. The EPA urban driving profile [10] provides a realistic discharge test, consisting of a power load which varies every second However, most battery tests, including the ones reported here, are conducted under constant-current or constant-power conditions, which are more appropriate for load-leveling applications.

Unlike the discharge modes, there is no fundamental limitation on the type of possible charge modes that might be used for a battery Constant-current charge is popular because it is easily implemented, but the Zn/NiOOH cell exhibits gas evolution and a rising Zn electrode overpotential at the end of a constant-current charge, unwelcome dendrite growth can be the result. Constant-voltage charging limits this excessive overpotential, but the resulting low currents at the end of charge lead to longer recharge times The methods of charging evaluated in the present experiments were a variety of pulse-charging modes in which the current rapidly varies between a high value (*on*) and a low or zero value (*off*).

Pulsed-current charging of Zn/NiOOH cells

Only recently has pulsed current been systematically evaluated as an alternative charging method for Zn/NiOOH cells, although it has long been known to improve the characteristics of electroplated deposits of various metals [11] Romanov [12] used alternating current superimposed on direct current to demonstrate a reduction in the number of Zn dendrites in alkaline Zn/NiOOH and Zn/AgO batteries The best results were obtained for pulsed currents having a sufficiently long off-time or sufficiently low frequency (<250 Hz) Chin *et al* [13] studied the effects of 60 Hz pulsed current on the deposition of Zn from an acid zinc chloride solution They found that the application of pulsed currents produced an increased number of nucleation sites and therefore more-uniform deposits. It is believed that a high-current peak creates a large surface overpotential, thereby increasing the number of nucleation sites and reducing the opportunity for dendrite formation [14] During the rest period following the current peak, local Zn concentration gradients can relax by diffusion of Zn species into the depleted diffusion layer, which prevents the development of excessive concentration overvoltage, hydrogen evolution, and dendrite growth

Smithrick [15] conducted pulse-current charge tests on Zn/NiOOH cells at frequencies of 120 - 1000 Hz He was unable to demonstrate that any pulse-charging method improved cell cycle life over that associated with constant current Investigations by McBreen [16] and his co-workers on the effects of pulse-charging on pasted Zn electrodes may explain why Smithrick observed no cycle-life improvement McBreen found that the advantages of pulse-charging were eliminated by double layer effects at frequencies much greater than 15 Hz At frequencies of 5 - 15 Hz, Zn was uniformly deposited close to the current-collector grid Wagner [17, 18] found 5 - 8 Hz to be optimum for improving Zn/NiOOH cell cycle life, and he also determined the

best rest-pulse ratio to be 3 1. Cells charged using this method had better capacity retention and less shape change. However, the discharge conditions utilized by Wagner were not so severe as those expected in demanding applications such as electric vehicles, since the depth-of-discharge was only about 50% based on the theoretical capacity of the NiOOH electrode

Appelt and Jurewicz [19], and Binder and Kordesch [20] have employed a 3-component pulse-charging method operating at 50 Hz to extend the cycle-life of the Zn electrode Beneficial peak current densities (pcd) of 5 - 15 mA cm^{-2} have been identified by Binder and Kordesch [20] for pulse-charging a Zn electrode having a Cu wire grid current collector. During the last two decades many other researchers have reported investigations on the use of pulse-charging for Zn electrodes [21 - 29].

The aim of the present work is to assess the effect of various pulse-charging regimens on the cycle-life performance of Zn/NiOOH cells operated under demanding 100% depth-of-discharge profiles Among the pulse-charging modes selected was an 8.3 Hz, 30 ms *on*/90 ms *off*, 15 mA cm^{-2} pcd regimen, which the research cited above, along with other studies [21 - 26], would suggest to be nearly optimal.

Experimental procedures

Cell case and electrode pack

The cell cases were constructed from polymethylmethacrylate, based on a design described by Nichols *et al* [6]. Figures 1 and 2 show the cell

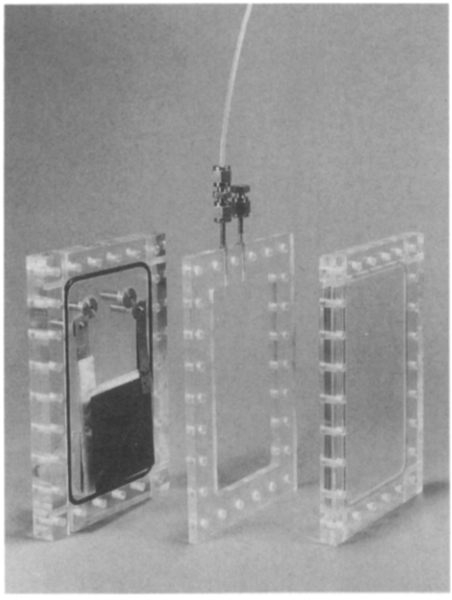

Fig 1 Zn/NiOOH cell, disassembled

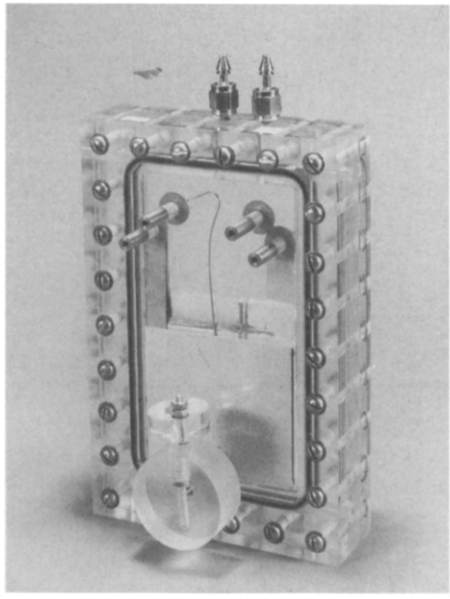

Fig 2 Zn/NiOOH cell, assembled

case in disassembled and assembled form, respectively. The central portion of the cell case determined the space in which the electrode pack must fit. Spacers made of various thicknesses of polyethylene sheets were added to the cell pack to produce an effective compression pressure of 27.6 kPa. The complete electrode pack consisted of a Zn electrode surrounded by a wick, enclosed with a separator wrap and placed between two NiOOH electrodes, each of which was surrounded by a wick. Two of the cells had a slightly modified electrode pack, which is described below. All materials were chosen for their ability to resist attack by concentrated alkaline solutions.

Zinc electrodes

Some experiments employed polymer-bonded Zn electrodes provided by Energy Research Corporation (Danbury, CT). These electrodes were first X-rayed, and then the most uniform were selected for experiments. Their dimensions were 6.2 cm × 7.0 cm and 0.61 mm thick, and the current collector consisted of 0.063 mm thick copper foil with 0 046 mm lead plating. Attached to the current collector was an Ag tab 0 127 mm thick, 4.3 cm × 0 9 cm. The current collector was covered with electrode material consisting of 95 wt.% ZnO, 2 wt.% PbO and 3 wt % polytetrafluoroethylene. A possible drawback of using a Cu foil current collector (instead of a mesh type) is that the Zn material on one side of the electrode is electrochemically inaccessible from the other. The electrode can therefore have two faces acting independently of each other

Other experiments repeated the tests previously conducted with foil current collectors, but with a copper mesh* current collector spot-welded to a copper tab. These Zn electrodes were prepared in our laboratory from a slurry which was vacuum-filtered to produce cakes which were bonded to each side of the Pb-plated Cu mesh. The composition of these electrodes was similar to those in the first set of experiments· 94 wt.% ZnO, 2 wt % PbO, 4 wt.% PTFE. The design capacity of all the Zn electrodes ranged from 30.8 mA h cm^{-2} to 38.1 mA h cm^{-2} Porosities, based on Zn metal, were 60% for the first (foil current collector) set of experiments and 75% for the second (mesh current collector) set.

NiOOH electrodes

The Ni electrodes** were sintered-Ni plaque, chemically impregnated with $Ni(OH)_2$ on a Ni mesh, which was welded to Ni tabs. Dimensions for the positive electrodes were 6.2 cm × 7.0 cm × 0 48 mm thick. The capacity was matched as closely as possible to one-half the design capacity of the mated Zn electrode, and two NiOOH electrodes were used in each cell pack.

---

*Exmet Corp , Bridgeport, CT, mesh 3Cu 6-4/O

**Eagle-Picher Industries, Inc , Colorado Springs, CO

Electrolyte

The composition of the electrolyte was 31 wt % KOH* (major impurity 0 04% K_2CO_3) and 1 wt.% LiOH**. An amount of ZnO in excess of saturation was added, and the solution was stirred for one week The electrolyte was stored in a polyethylene bottle with an attached CO_2 scrubber.

Separator and wicks

A wick consisting of one layer of Aldex paper*** surrounded the Zn electrode and served to keep the electrode together and supply it with a reserve of electrolyte The separator wrap consisted of the following layers (listed beginning with the layer closest to the Zn electrode):

(i) 1 layer of microporous polypropylene, Celgard 3500†;

(ii) 1 layer of cellophane, PUDO-193††,

(iii) 1 layer nickelized polypropylene, Celgard K317† with the nickelized face toward the Zn electrode,

(iv) 1 layer of microporous polypropylene, Celgard 3500†

Wagner *et al* described the benefits of using this separator system.

The second set of experiments (with Zn electrodes using a Cu mesh current collector) had a simpler separator system consisting of three layers of Celgard 3401† microporous polypropylene. The wicks adjacent to the Ni electrodes were non-woven nylon, Pellon 2502K4†††, and their purpose was to keep the Ni electrodes supplied with electrolyte through capillary action.

Reference electrode and cell preparation

A platinum wire dipped in Hg/HgO in equilibrium with 31% KOH provided a stable reference potential. It was mounted in a polymethylmethacrylate cell that screwed into the special compartment on one side of the cell case, as shown in Fig. 2. The reference electrode maintained electrolytic contact with the main cell through a 0.5 mm capillary drilled through one face of the cell case. When the cell pack was ready for assembly, it was placed in the cell housing with the appropriate spacers. The cell was then compressed with screws around its perimeter until the O-rings filled their machined grooves and all three sections of the cell case contacted each other. After vacuum leak testing, the evacuated cell was filled with electrolyte through one of its two upper ports while the other port was sealed Electrolyte was drawn to a level 1 cm above the top of the cell pack, and the reference electrode compartment also filled with electrolyte. A CO_2 scrubber was attached to one of the ports at the top of the cell; the other one was sealed.

---

*J T Baker Chemicals Co , Phillipsburg, NJ

**Matheson, Coleman and Bell, Manufacturing Chemists, Norwood, OH

***Aldex Company

†Celanese Fibers Corp , Summit, NJ

††E I duPont de Nemours, Inc , Wilmington, DE

†††Pellon Corp , Chelmsford, MA

TABLE 1

Cell specifications and cycling parameters

Cell*	Const I, 4A	Const I, 4B	8 3/8 3 8 4	30/90 16A	30/90 16B	30/90 16C	30/90 30A	30/90 30B	10/90 41A	10/90 41B
Design capacity (A h)	1 52	1 65	1 55	1 49	1 46	1 62	1 34	1 42	1 51	1 52
(Theoretical Zn capacity)/ (Theoretical NiOOH capacity)	3 15	3 02	3 21	3 00	3 01	2 94	2 77	2 95	3 12	3 14
Electrolyte/ A h (g)	8 1	8 6	7 1	8 5	7 3	8 8	8 6	7 1	7 7	8 8
Frequency (Hz)	Const curr	Const curr	60	8 3	8 3	8 3	8 3	8 3	10	10
Off-time/ On-time	Const curr	Const curr	1	3	3	3	3	3	9	9
Charge time (h)	4 5	5 0	4 5	4 5	4 5	5 0	2 25	2 25	4 5	4 5

*The cell is designated by on time (ms)/off time (ms), peak current density (p c d) in mA cm^{-2}

Cell specifications

The specifications of the cells are given in Table 1 The design capacity is based on one-third of the total ZnO capacity present in the negative electrodes. The Ni electrode theoretical capacity was matched as closely as possible to the Zn electrode design capacity, *i e* , the total Zn capacity was close to 3.0 times the theoretical NiOOH capacity.

NiOOH electrode formation

Each cell received three "formation" cycles by being charged for 20 h at the 10 h rate (current = design A h/10 h) and then discharged at the 3 h rate (current = design A h/3 h) until the cell voltage reached zero. The Ni electrodes evolved oxygen during the second half of the charge and evolved hydrogen during the second half of the discharge, so water was subsequently added to compensate for such losses. During the third discharge, the current was gradually reduced to about 50 mA to extract the remaining capacity of the Zn electrode. Finally, the cell was charged for 20 h at the 10 h rate to establish the appropriate quantity of metallic Zn, and then it was placed on a regular cycling regimen.

Cycling conditions

The computer-controlled mutiple-channel system for cell cycle-life testing is described by Katz *et al* [30, 31]. Its eight independent current

controllers (each capable of operating two series-connected cells) are driven by separate charge and discharge power supplies. With a response time of 1 ms, they can accept an external square-wave signal and pulse-charge the cell according to the parameters set by this signal. Routine monitoring and recording of electrode overpotentials and cell voltages and currents was performed with an LSI 11/23 microcomputer* A mismatch of impedances between the electrode terminals and the reference electrode prevented the accurate measurement of overpotentials during pulse-charging.

Various pulse-current charging profiles were compared with the constant-current mode for their effects on cycle life. All cells were cycled with the same discharge conditions, *i e* , a constant power of about 1 0 W, with a cutoff voltage of 1.0 V. The power level for each cell was based on a discharge time of 2.5 h, the Ni electrode capacity, and the average cell voltage during the last formation cycle. Thus the cells were effectively cycled at 100% depth-of-discharge. Thirty-minute open-circuit periods were provided at the end of each half-cycle Table 1 provides details of the charge half-cycle for each cell

A 4% overcharge was applied each cycle to compensate for the inefficiency of the NiOOH electrode, as it evolves oxygen during charging. Within 20 - 50 cycles this overcharging of the Zn electrode resulted in a loss of ZnO reserve, as indicated by a sharp rise in the Zn electrode overpotential near the end of charge The ZnO reserve was then restored by fully discharging the cell to 0.0 V This was followed by a "formation" charge half-cycle to establish a Zn reserve, after which regular cycling was resumed.

Paired cells on a common cycling regimen were cycled in series until a significant difference in their capacities developed, after which time the cells were cycled separately. Testing continued for 125 cycles or until the cell capacity fell below 60% of its original value or shorting occurred Voltage measurements include.

(i) cell voltage at current-on and current-off during pulse charging;

(ii) cell voltages and electrode potentials *versus* Hg/HgO reference during constant-current charge, constant-power discharge, and/or on open circuit.

Table 1 summarizes the cell cycling conditions.

Post-cycling tests

The Zn electrodes were visually examined after cycling to determine the extent of Zn redistribution and dendritic penetration of the separators Zinc redistribution was determined more precisely by obtaining an X-ray** image of the Zn electrode and estimating the percentage of the total area of the electrode face (front and back) which lacked Zn deposits Additional tests were performed on selected electrodes, including scanning electron

*Digital Equipment Corporation, Marlboro, MA

**CGR Medical Corp , Baltimore, MD , Model 55

microscopic (SEM) examination* and dissolution of Zn species from the Ni electrodes (using concentrated nitric acid followed by atomic absorption analysis for Zn content) Plots of capacity and coulombic efficiency *versus* cycle number, and voltage *versus* time plots for specific cycles, were obtained using the computer's data-reduction software.

Results and discussion

Important pulse-charging variables to consider in evaluating the performance of these cells include the frequency, on/off time ratio, off-time, and peak current density (pcd) As explained earlier, a high current density can increase the number of nucleation sites for the charge reaction on the Zn electrode, thereby reducing dendrite initiation. However, an unwanted side effect may be inefficient operation of the Zn electrode. A sufficiently long off-time improves the mass transfer conditions for the reaction by allowing Zn ions to diffuse into the depleted diffusion layer, thereby reducing dendrite growth. An examination of Table 2, the cell cycle-life performance data, shows that the last seven cells have the same off-time, 90 ms, and nearly the same frequency, 8 3 Hz - 10 Hz With these two variables fixed, the on/off ratio and pcd's for these cells are directly linked to each other Focusing our attention on cell performance as a function of pcd for all the cells allows us to make some useful comparisons.

Effect of pcd

High-pcd cells failed early; the best achieved a useful cycle-life of 43 cycles. Low-pcd cells performed better, achieving a maximum useful life of 90 cycles The intermediate-pcd cell using a 30/90 pulse generally performed best, reaching 120 cycles maximum with significant useful capacity still remaining.

Compare the cycle-life capacity performance shown in Fig. 3 for Cells Const I, 4A, 30/90, 16A, and 10/90, 41B which are low, medium and high pcd cells, respectively Cell 30/90, 16A had a stable capacity throughout most of its cycle life, as did Cell Const I, 4A until shorting occurred. The initial capacity decline of Cell 30/90, 16A was halted by gradual adjustment of the overcharge, up to 7%. Cell Const. I, 4A stayed above 75% of design capacity for about 90 cycles The ZnO reserve was recovered twice, and after the second time (cycle 75) the capacity declined rapidly Cell 10/90, 41B was connected in series with Cell 10/90, 41A, which started losing capacity at cycle 21 However, the capacity of Cell 10/90, 41B continued to drop, and re-establishment of the ZnO reserve at cycle 56 did little to arrest its decline

*American Metals Research, Inc , Bedford, MA, Model 1000

TABLE 2

Cell cycling performance data

Cell*	Const I, 4A	Const I, 4B	8/8, 8	30/90, 16A	30/90, 16B	30/90, 16C	30/90, 30A	30/90, 30B	10/90, 41A	10/90 41B
Charge peak current density (mA cm^{-2})	4 5	3 9	8 4	15 5	15 5	15 7	30 1	30 1	40 6	40 6
Cycles above 75% capacity (total no cycles)**	90(100) N	74(77) N	50(107) N	107(107) N	55(79) Z	120(125) N	43(76) N	31(61) Z	20(25) Z	34(88) Z
Capacity loss per cycle (%)	0 49	0 66	0 30	0 21	0 52	0 21	0 71	1 00	2 72	0 78
Area loss per cycle (%)	0 25	0 85	0 18	0 17	0 42	0 41	0 39	0 52	0 48	0 35
Major mode of decline	Zn dendrite shorting	Zn dendrite shorting	Zn dendrite shorting	Zn shape change	Zn dendrite shorting	Zn shape change	Low Ni electrode efficiency	Zn dendrite shorting	Zn dendrite shorting	Zn dendrite shorting

*The cell identity is designated by on time (ms)/off time (ms), pcd (mA cm^{-2}, rounded)
**N = nickel electrode limiting at end of test Z = zinc electrode limiting at end of test

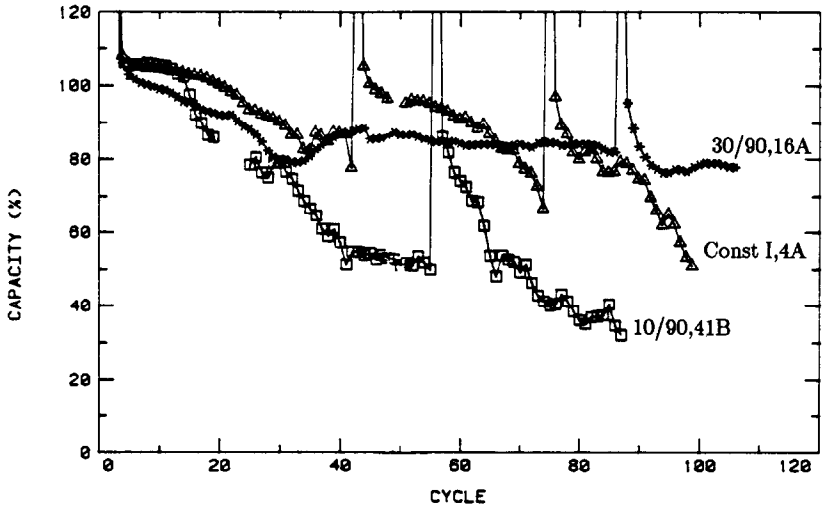

Fig 3 Capacity *vs* cycle number for Cells Const I, 4A (△), 30/90, 16A (*), 10/90, 41B (□) All identification and cycling conditions are given in Table 1 The cells are discharged to a 1 V cutoff Peaks in the data indicate discharges to re-establish the ZnO content of the negative electrode

Low pcd cells

Both constant-current charged cells showed evidence of shorting; dendrites penetrated the upper edge of the separator of Cell Const I, 4B between cycles 50 and 60 followed by a rapid decline in cell capacity Cell Const I, 4A probably had insufficient reducible ZnO by cycle 20, as indicated by a larger-than-expected open-circuit potential difference (—1 4 V *versus* Hg/HgO for the Zn electrode) This condition gradually led to Zn dendrite growth until shorting occurred. At that point, the capacity displayed a sharp decline, even after re-establishing the ZnO reserve

Figure 4 shows charge–discharge voltage plots for Cell Const I, 4A at cycles 10 and 73. A short occurred at cycle 73, confirmed by examination of the separator and wicks after termination of the cycling Several spots of Zn were visible on the wicks, and the inner layers of the separator appeared to contain some Zn material. In addition, the nickelized layer of the separator was partly separated from its polypropylene support

The capacity *versus* cycle-number curves of Cell 8/8, 8, the square-wave 60 Hz cell, and Cell 30/90, 30B, whose performance is discussed later, are compared in Fig 5 Cell 8/8, 8 retained a capacity greater than 75% of its design value for about 50 cycles, but after a second ZnO reserve recovery at cycle 57, it displayed a rapid capacity decline At cycle 68, the overcharge was increased to 20%, and then retained at 10% for the next 25 cycles the cell did regain some capacity, but did not reach its original level. This cell also had dendrite shorting

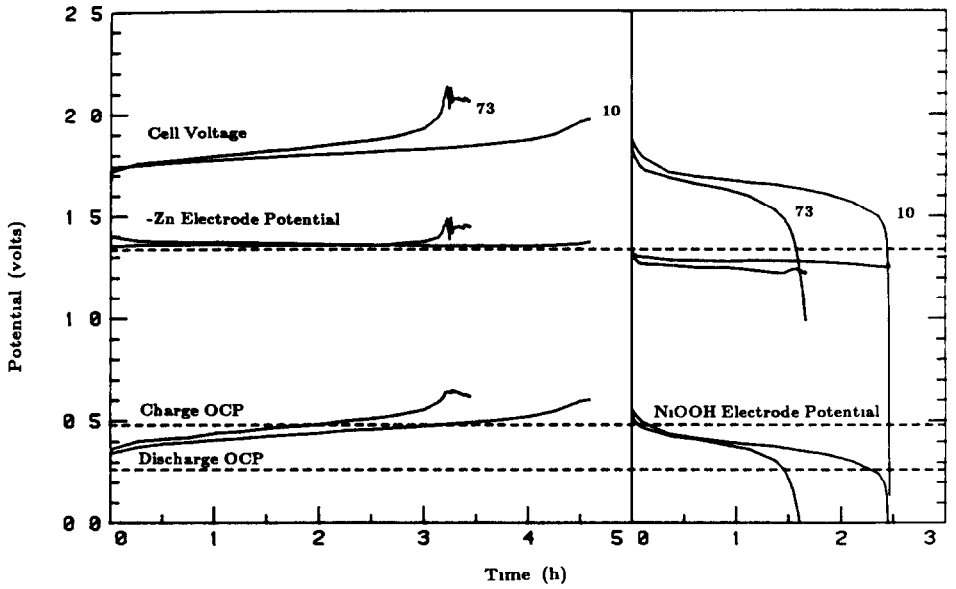

Fig 4 Cell voltage and electrode potentials, cycles 10 and 73, Cell const I, 4A Charge left portion of graph, discharge right portion of graph, constant current, 4 mA cm^{-2} Electrode potentials are relative to Hg/HgO ——, Cell voltage and electrode potentials, - - - -, open-circuit electrode potentials

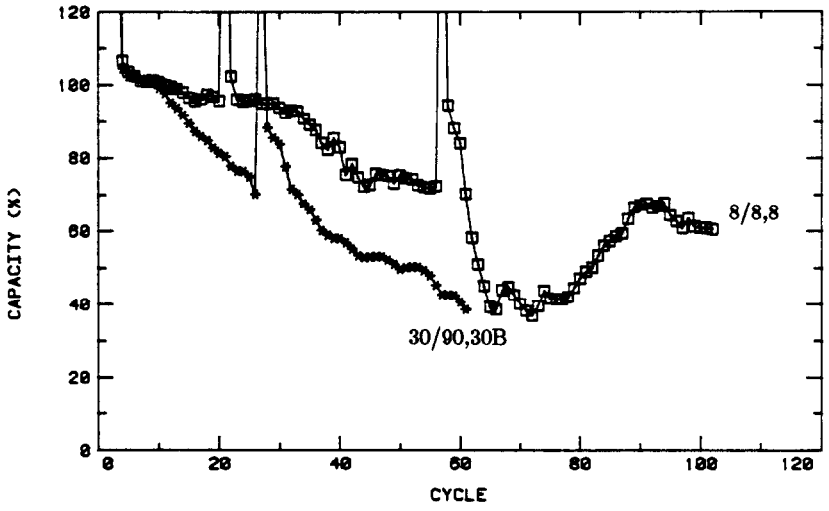

Fig 5 Capacity *vs* cycle number for Cells 8/8, 8 (□) and 30/90, 30B (*) Specifications as Fig 3

Medium pcd cells

Zinc electrodes cycled with the medium-pcd, 30/90, 16 pulse-charging mode, had a lower rate of capacity loss and sustained longer periods between required ZnO formation cycles than all other cells Figure 6 compares cycle-

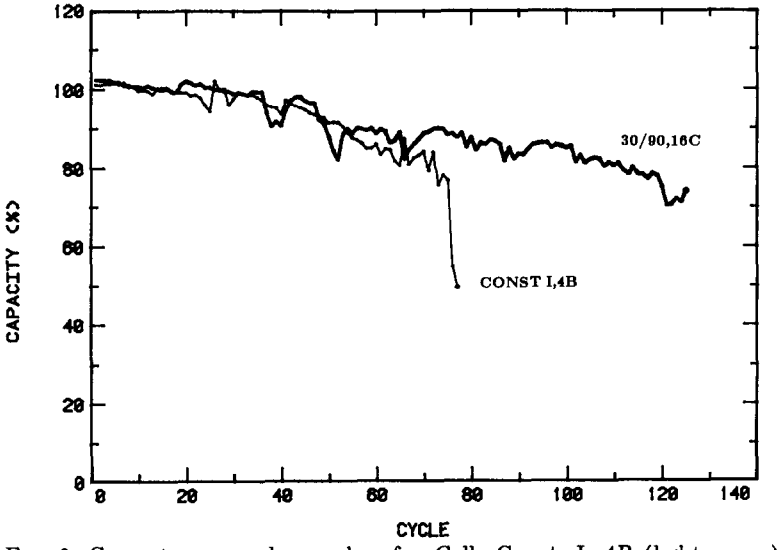

Fig 6 Capacity *vs* cycle number for Cells Const I, 4B (light curve) and 30/90, 16C (heavy curve)

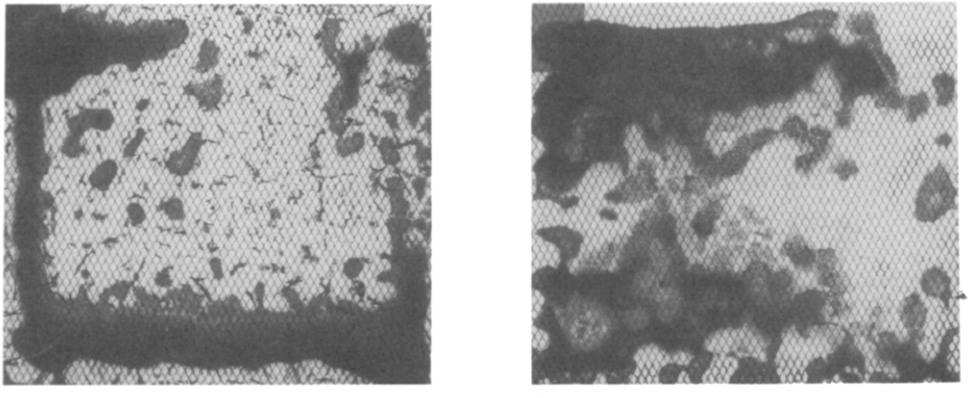

(a) (b)

Fig 7 X-ray images of Zn electrode after cycling for Cells Const I, 4B (a) and 30/90, 16C (b)

life performance for the second set of experiments using Zn electrodes prepared on copper-mesh current collectors. Cell Const I, 4B and Cell 30/90, 16C exhibit nearly equivalent performance until cycle 50, at which point the capacity of the low-pcd Cell Const I, 4B declined and it eventually shorted at cycle 77, whereas Cell 30/90, 16C continued to perform well until it was removed for analysis after cycle 125 X-ray photographs of the Zn electrodes (Fig. 7) for these two cells revealed significantly more area loss for the constant-current, low pcd cell *versus* the 30/90, 16C pulse-charged medium-pcd cell

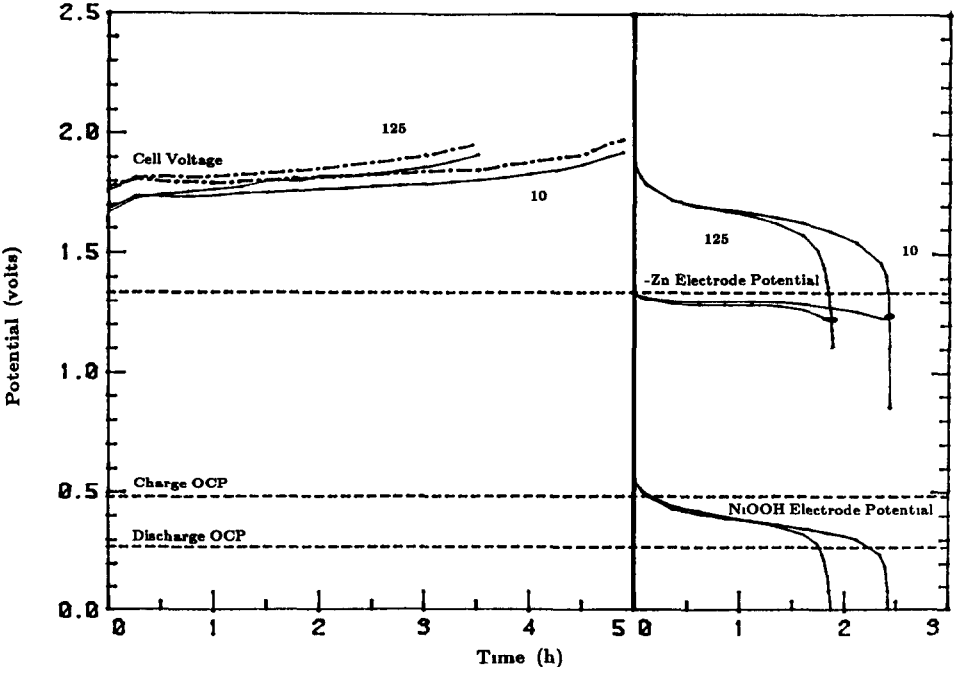

Fig 8 Cell voltages and working electrode potentials, cycles 10 and 125, Cell 30/90, 16C Charge left portion of graph, — — cell voltage measurements at current on, —— cell voltage measurements at current off Discharge Right portion of graph Other notations are as in Fig 4 Note that the (pulsed-charged) electrode potentials are not shown

Cell voltages and working electrode voltages *versus* Hg/HgO reference *versus* time are presented for Cell 30/90, 16C, cycles 10 and 125 in Fig. 8 The dot–dash line for the cell voltage on charge represents the potential during the "on" part of the charging pulse: the solid line represents cell voltage during the "off" part. The cell voltage charging curves are slightly irregular, especially for cycle 125, perhaps indicating high-resistance shorts By cycle 40, dendrites were observed on the edges of the separator; however, post-cycling examination of these separator edges did not show any breaks in the separator seals. Dendritic shorting appears not to have seriously compromised the performance of this cell Very high overpotentials at the end of charge are not formed by cycle 125, and this cell still had adequate cycling capacity left at that time

High pcd cells

The high-pcd Cell 10/90, 41B performed poorly compared with Cells Const I, 4A and 30/90, 16A. The Zn electrode potential (measured at open circuit after charge) reached −1 4 V (*versus* Hg/HgO) after only 10 cycles. Between cycles 10 and 20, the cell lost approximately 20% of its capacity, and the charge–discharge curves indicated that this decline might be related to cell shorting The occurrence of shorts was corroborated by post-test

examination of the separator and wicks. Cycles 20 to 39 showed low overpotential for the Zn electrode on charge After cycle 35, the Zn electrode became capacity-limiting on discharge After cycle 40, this limitation was coupled with a rise in the Zn overpotential on charge. Figure 9 shows two cycles for this cell cycle 15 (high overpotential on the Zn electrode during charge, with shorting toward the end of charge), and cycle 40 (high overpotential during both charge and discharge). It is not surprising that a cell at high-pcd can develop problems with its Zn electrode, even quite early in life Shorting was clearly one problem, but other mechanisms may have contributed to Zn electrode capacity-limiting behaviour

(i) a larger amount of hydrogen evolution could have resulted in loss of metallic Zn reserve,

(ii) dendrite growth stoppage either by the separator or by current interruption could lead to isolation of Zn metal from the current collector The separator was in very poor condition, the nickelized layer had peeled from its support, and the inner layers appeared to be heavily loaded with Zn material This last observation provides support for the second mechanism of capacity loss

It was straightforward to calculate the "resistance" of the cells which were pulse-current charged (30/90, 16A and 10/90, 41B), since the computer measured the cell voltage immediately prior to current interruption and within 100 ms after current interruption. No comparable measurements were available for the constant-current cells At cycle 30 the resistance of Cell 30/90, 16A was 12 mΩ and that of Cell 10/90, 41B was 28 mΩ (both measured at the end of charge). At cycle 69, the values were 2.8 and 4.5 mΩ, respectively Note that these measurements include activation overpotentials

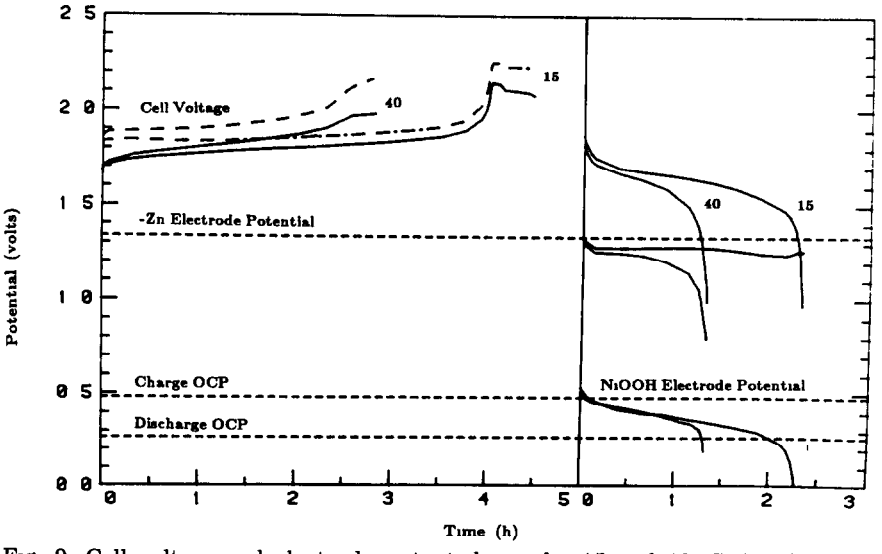

Fig 9 Cell voltage and electrode potentials, cycles 15 and 40, Cell 10/90, 41B Other notations are as in Fig 8

and ohmic losses, but mass-transfer overpotentials should be excluded, because they relax more slowly Plausible explanations for voltage differences between charge curves are·

(i) higher non-ohmic potential drop due to higher pcd in Cell 10/90, 41B,

(ii) higher ohmic resistance (due, for example, to bubbles of evolved gas);

(iii) higher activation overpotentials.

The Cell 30/90, 30B experiment was intended to investigate a charging regimen intermediate between those of Cell 30/90, 16A and Cell 10/90, 41B The profile was the same as that employed for Cell 30/90, 16A, but with twice the current density Cell 30/90, 30B behaved in a manner quite similar to that of Cell 10/90, 41B, and its rate of capacity decline was slightly higher (Fig 5). As was the case for Cells 10/90, 41A and 10/90, 41B, Cell 30/90, 30B rapidly became limited on discharge due to a high overpotential at the Zn electrode. Cell 30/90, 30B exhibited even higher voltages on charge than Cell 10/90, 41B. This can be explained by the fact that Cell 30/90, 30B passed more than twice the number of coulombs at current-on, for the same 90 ms current-off time Another Cell, 30/90, 30A, with the same charging regimen as 30/90, 30B, displayed peculiar behavior its Zn electrode was never limiting (neither on charge nor on discharge), and it is suggested that the Ni electrode exhibited anomalously low efficiency.

Foil versus mesh current collectors

Two different types of current collector were used for the Zn electrodes — copper foil and copper expanded mesh. Rates of capacity loss were similar for both types of current collector, whereas rates of Zn material area loss were generally greater for the mesh than for the foil collector. Binder and Kordesch [20] found superior performance for mesh collectors compared with foil collectors, which they attributed to better mechanical anchorage of the Zn deposit on the mesh substrate Our longest-lived Cell, 30/90, 16C, had a mesh collector. SEM examination (Fig 10) reveals that pulse-charged electrodes have Zn deposits with smaller particle sizes than those charged with constant current, for both foil and mesh collectors

In the cells that employed foil current collectors, nickelized Celgard and cellophane separators were used, whereas the cells that utilized mesh current collectors contained only microporous polypropylene (Celgard) separators Reduced rates of Zn redistribution were found for the foil-collector cells, but the nickelized separator material did not appear to have arrested dendrite penetration The benefit of nickelized separators for restricting Zn anode thickness growth in pulse-charged cells is cited by Wagner *et al* [27]. Sato *et al* [32] achieved long cycle-life with PVA-coated Dynel separators

The medium-pcd Cell 30/90, 16A used a copper-foil current collector, and it performed as well as the comparable Cell 30/90, 16C with copper-mesh current collector For Cell 30/90, 16A the Zn *versus* Hg/HgO reference

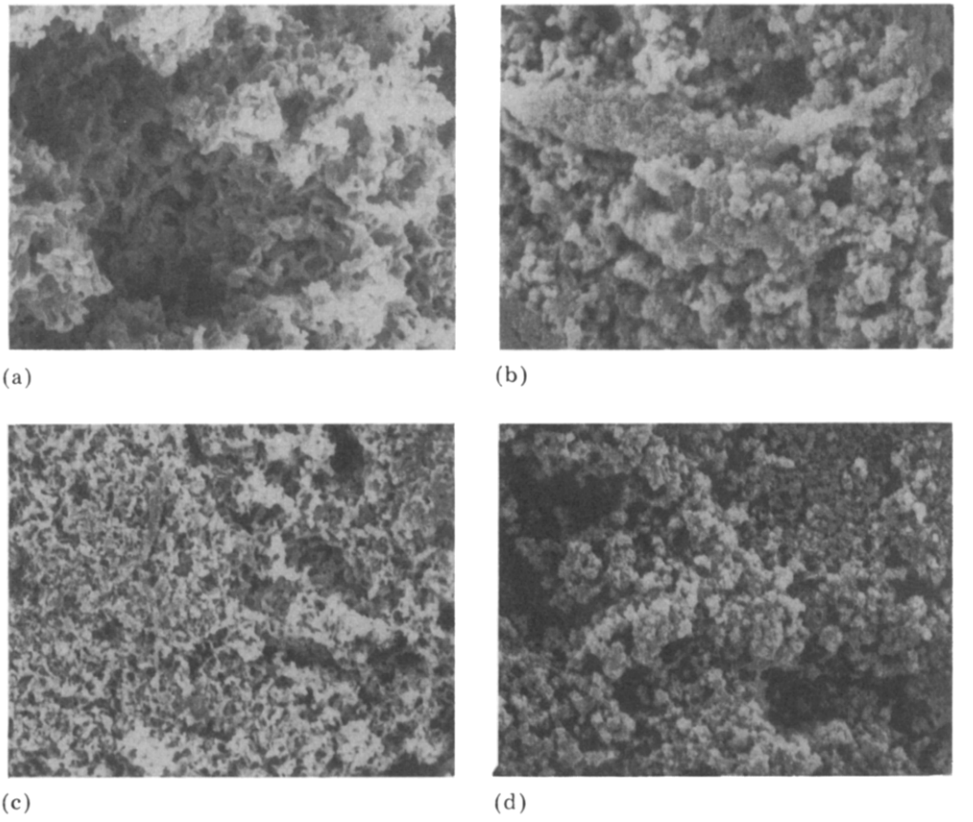

Fig 10 SEM photographs of Zn electrodes after cycling in constant-current and 30/90, 16 pulse-charged cells (×2000) (a) Const I, 4A, (b) Const I, 4B, (c) 30/90, 16A, (d) 30/90, 16C

potential (measured at open circuit during charge) reached −1.4 V after 62 cycles, which was much later than observed for cells cycled with constant current Two explanations are proposed:

(i) the ZnO reserve required more time to diminish because of an increase in hydrogen evolution rates during charge (the current density was equal to four times that employed at constant current). This phenomenon would prevent the Zn electrode from operating at 100% efficiency.

(ii) a small ZnO reserve and a 16 mA cm^{-2} pcd, with a 90 ms rest time after each pulse allowed relaxation of concentration gradients and improved mass transfer characteristics at the Zn electrode.

On discharge, Cell 30/90, 16A was never limited by its Zn electrode Its separator was in good condition at the end of cycling, no Zn was detectable in the inner layers, and no traces of shorts were visible. Another cell, 30/90, 16B, using the same charging regimen and a copper-foil current collector failed to match the performance of Cells 30/90, 16A and 30/90, 16C. Its life ended with dendritic shorting by cycle 79, possibly due to faulty

separator seals Cell 30/90, 16A never showed evidence of shorting or excessive overpotentials.

Zn transport to the NiOOH electrode

A Zn material balance was obtained for the cells with mesh current collectors, using atomic absorption analyses. In these cells, 98% of the Zn was accounted for, and the distribution of Zn was nearly the same for Cells Const I, 4B and 30/90, 16C. Figure 11 illustrates the average Zn distribution before and after cycling for these cells. It can be seen that over 20% of the original Zn has migrated to the NiOOH electrode. Using additional data from several similar cells (not reported in detail here) that were cycled in the constant current or pulse-charged modes for 2 - 110 cycles, a plot of the mass of

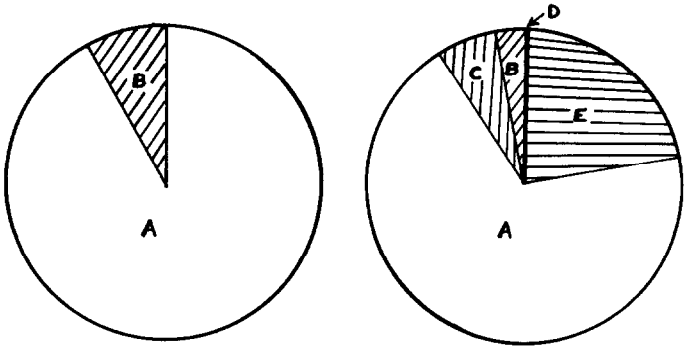

Fig 11 Average Zn distribution for both Cells Const I, 4B and 30/90, 16C before and after cycling Before cycling A Zn electrode, 91 9%, B electrolyte, 8 1% After cycling A Zn electrode, 68 8%, B electrolyte, 3 2%, C cell washes, 6 2%, D wicks, 0 3%, E Ni electrode, 21 5%

Zn found in the Ni electrode *versus* the number of cycles was made, and the data were subjected to linear regression analysis with the results shown in Fig. 12. The amount of Zn found in the Ni electrode after cycling was highly correlated (r = 0 89) with the number of cycles. The amount of Zn found in the NiOOH electrode after only a few cycles was over 800 mg, or more than half that found after more than 100 cycles A large amount of the Zn transport therefore occurs very early in the life of the cell.

Conclusions

There is a clear trend toward increased cycle life with decreasing peak current density for the pulse-charged cells. This result is consistent with that of McBreen *et al* [33]. The greater faradaic conductance and increased number of nucleation sites promotes fine Zn deposits close to the current collector. Superior cycle-life performance was obtained using a pulse-charging mode of 30 ms on/90 ms off and 16 mA cm^{-2} peak current density. The

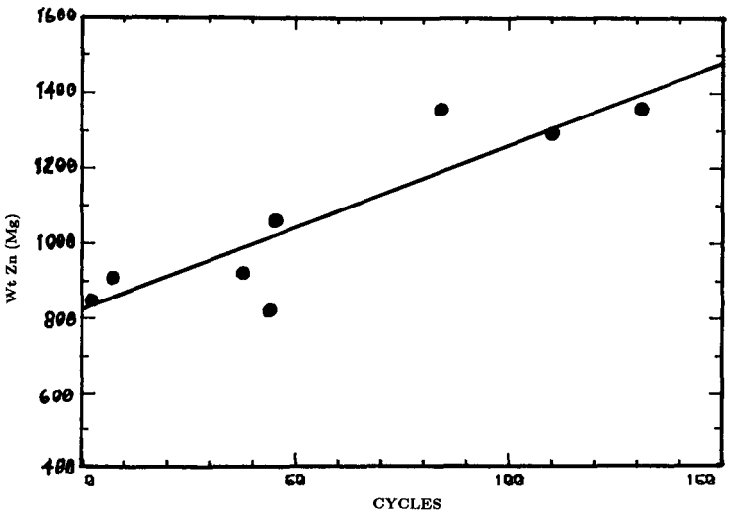

Fig 12 Amount of Zn deposited in the Ni electrode *vs* number of cycles

60 Hz pulse-charged Cell 8/8, 8 exhibited poor cycle life, probably because of an insufficient relaxation time in the current-off portion of the profile. The results of McBreen *et al* [33] indicate that 50 ms are required to discharge the double-layer in a half-charged Zn electrode, and that the best results are expected at frequencies of 10 Hz or less. Dendritic shorting is associated with high overpotentials and greater rates of capacity loss than area loss in many of these cells Cell 30/90, 16C, the longest-lived, exhibited no shorting, and no high overpotentials were observed for this cell during charging The present results were obtained with cells cycled at 100% depth-of-discharge (DOD) and should not be compared directly with cells cycled at 80% DOD or less (*e g* , Wagner [27]) The substantial amount of Zn transported to the Ni electrode early in the cycle life of these cells is an interesting phenomenon which requires further study.

Acknowledgements

This work was supported by the Assistant Secretary for Conservation and Renewable Energy, Office of Energy Storage and Distribution, of the U.S Department of Energy under Contract No DE-AC03-76SF00098

The authors also thank Energy Research Corporation for providing some of the Zn electrodes

References

1 E J Cairns and E H Heitbrink, Electrochemical power for transportation, in J O'M Bockris, B E Conway, E Yeager and R E White (eds), *Comprehensive Treatise of Electrochemistry*, Vol 3, Plenum Publishing Co , New York, 1981, p 421

2 A Himy, *Proc 16th Intersoc Energy Conv Eng Conf*, American Society of Mechanical Engineers, New York, 1981, p 645

3 J McBreen and E J Cairns, The zinc electrode, in H Gerischer and C Tobias (eds), *Advances in Electrochemistry and Electrochemical Engineering*, Vol 10, Wiley–Interscience, New York, 1978, p 273
4 R Jain, F R McLarnon and E J Cairns, *Paper No 84, 168th Meet of the Electrochemical Society*, Las Vegas, NV, The Electrochemical Society, Pennington, NJ, 1985
5 E G Gagnon, *J Electrochem Soc , 133* (1986) 1989
6 J T Nichols, F R McLarnon and E J Cairns, *Chem Eng Commun , 37* (1985) 355
7 J T Nichols, F R McLarnon and E J Cairns, Active material redistribution on rates in zinc electrodes, *Lawrence Berkeley Lab Rep No LBL-17397, 1983*
8 R F Thorton and E J Carlson, *J Electrochem Soc , 127* (1980) 1448
9 J McBreen, in J O'M Bockris, B E Conway, E Yeager and R E White (eds), *Comprehensive Treatise of Electrochemistry*, Vol 3, Plenum Publishing Co , New York, 1981, p 303
10 Environmental Protection Agency, Urban Driving Profile, Federal Register, 1970
11 N Ibl and F Leaman (eds), *American Electroplaters Society 2nd Int Symp on Pulsed Plating, 1980*
12 V Romanov, *Zh Prikl Khim , 34* (1961) 2692
13 D -T Chin, R Sethi and J McBreen, *J Electrochem Soc , 129* (1982) 2677
14 D N Bennion, A review of membrane separators and zinc/nickel oxide battery development, *Final Rep Argonne Nat Lab , 1980*
15 J J Smithrick, *Proc 15th Intersoc Energy Conv Eng Conf*, American Institute of Aeronautics and Astronautics, New York, NY, 1980, p 1203
16 J McBreen, in J McBreen, D -T Chin, R S Yeo and A C C Tseung (eds), *Proc Adv in Battery Materials and Processes*, The Electrochemical Soc , Vol 84-4, 1984, p 292
17 O C Wagner, High cycle life, high energy density nickel–zinc batteries, *Rep No 5, U S Army Electronics R and D Command, Fort Monmouth, NJ, 1982* See also *Rep No 3, 1980*
18 O C Wagner and A Almerini, *Proc 31st Power Sources Symp* , Electrochemical Society, Pennington, NJ, 1984, p 255
19 K Appelt and K Jurewicz, *J Power Sources, 5* (1980) 235
20 L Binder, *Ext Abstr 36th Meeting Int Soc Electrochem , 1985*, p 07270
21 G P Marchenko, *Vopr Khim Khim Tekhnol , 63* (1981) 32
22 Jos Hendryx, The zinc electrode, *Dissertatie Drukkerji*, Wibro, Helmond, The Netherlands, 1984
23 J E Oxley, *NASA Rep No ER-377*, Leesona Moos Laboratories, Great Neck, NY, 1966
24 V V Romanov, *Elektrokhimiya, 7* (1971) 1453
25 K Appelt and K Jurewicz, *Electrochim Acta, 27* (1982) 1701
26 S Arouete, K F Blurton and H G Oswin, *J Electrochem Soc , 116* (1969) 166
27 O Wagner, A Almerini and R L Smith, *Proc 29th Power Sources Conf*, The Electrochemical Society, Pennington, NJ, 1981, p 237
28 D T Chin and S Venkatesh, *J Electrochem Soc , 128* (1981) 1439
29 J J Smithrick, Effect of positive pulse charge waveforms on cycle life of nickel–zinc cells, *DOE-NASA/1044-79/13, 1979*
30 M H Katz, J T Nichols, F R McLarnon and E J Cairns, *J Power Sources, 10* (1983) 149
31 M H Katz, F R McLarnon and E J Cairns, Computer control of electrochemical experiments with application to zinc/nickel oxide cells, *Lawrence Berkeley Lab Rep No LBL-15546, 1982*
32 Y Sato, M Kanda, H Niki, M Ueno, K Murata, T Shirogami and T Takamura, *J Power Sources, 9* (1983) 147
33 J McBreen, E Gannon, D -T Chin and R Sethi, *J Electrochem Soc , 130* (1983) 1641